Neutron-induced reaction cross sections of selenium isotopes at 14−15 MeV: Activation measurements and covariance analysis

Vandana [1] Shivani Sharma[1] N. L. Singh[2†] Mayur Mehta[3] Mitul Abhangi[3,5] Ratnesh Kumar[3] Himanshu Sharma[3] Sudhirsinh Vala[3,5] R. K. Singh[4] R. J. Makwana[4] R. D. Chauhan[4] K. Katovsky[6] Pargin Bangotra[1‡]

[1]Nuclear and Atmospheric Research Laboratory, Department of Physics, Netaji Subhas University of Technology, Dwarka, New Delhi 110078, India
[2]Department of Nanotechnology, Delhi Skill and Entrepreneurship University, Dwarka, New Delhi 110077, India
[3]Institute for Plasma Research, Gandhinagar, Gujarat 382428, India
[4]Department of Physics, The Maharaja Sayajirao University of Baroda, Baroda, Gujarat 390002, India
[5]Homi Bhabha National Institute, Training School Complex, Anushaktinagar, Mumbai 400094, India
[6]Department of Electrical Power Engineering, Brno University of Technology, Brno 61600, Czech Republic

Abstract: Neutron-induced reaction cross sections of Se isotopes were investigated using the activation technique via ^{3}H(D, n)^{4}He (D-T) fusion reaction at the Neutron and Ion Irradiation Facility (NIIF) of the Institute for Plasma Research (IPR), India. The emitted gamma (γ) ray from a radioactive sample (Se) was examined using a High Purity Germanium (HPGe) detector. The measured cross sections of ^{76}Se(n, p)^{76}As, ^{78}Se(n, p)^{78}As, ^{82}Se(n, $2n$)^{81}Se^{g}, ^{76}Se(n, $2n$)^{75}Se, and ^{80}Se(n, α)^{77}Ge are 55.30 ± 4.09 mb, 18.77 ± 1.12 mb, 529.78 ± 51.23 mb, 903.98 ± 55.99 mb, and 2.01 ± 0.12 mb, respectively, at the neutron energy of 14.96 ± 0.22 MeV. The detailed uncertainty propagation from the various parameters and cross-correlation of the aforementioned reactions was estimated using covariance analysis. Furthermore, the measured cross sections were compared with the EXFOR database and evaluated nuclear libraries (ENDF/B-VIII.1, JEFF-4.0, JENDL-5, TENDL-2023 and CENDL-3.2). The cross sections were also reproduced theoretically using TALYS 2.0 code with an adjusted (optimized) set of parameters, and the contributions of various nuclear reaction mechanisms to the cross section were systematically analyzed and discussed. In addition, the measured reaction cross sections were quantified using various established semi-empirical systematic formulae. This study also performed statistical validation via chi-square minimization to identify the theoretical models and semi-empirical formulae that accurately reproduce the best measured cross section.

Keywords: selenium, activation technique, HPGe detector, covariance analysis, TALYS 2.0 code, semi-empirical systematic formulae

DOI: 10.1088/1674-1137/ae7a19 **CSTR:** 32044.14.ChinesePhysicsC.50104003

I. INTRODUCTION

The behavior of selenium (Se) is significant for evaluating the effectiveness of nuclear waste management as well as mobilization from the fuel matrix of spent nuclear fuel to the environment. Se is primarily produced as a fission product during the operation of nuclear fuel such as uranium-dioxide (UO_2). During reactor operation, Se also exists in the form of selenide ions (Se^{2-}) that substitute oxygen from the UO_2 lattice, forming strong bonds and sparingly soluble solid solution with the nuclear fuel matrix [1]. Furthermore, Se isotopes are predominantly employed in the healthcare sector and as nutrient in some refined food items. Through a neutron-induced reaction, ^{76}Se generates the residual nuclei ^{75}Se as a potential gamma (γ) source substitute of Ir-192 for brachytherapy [2, 3]. In addition, ^{77}Se and ^{78}Se are transmuted into the therapeutic radioisotope (^{77}Br) in the healthcare sector. However, the (n, p) reaction channel of Se produces arsenic (As) radioisotope that is toxic in nature. The production of As radioactive isotopes (^{72}As and ^{77}As) from the (n, p) reaction is exploited in medical diagnostics and therapies such as Positron Emission Tomography (PET) imaging. Moreover, a significant discrepancy in the previously reported data (EXFOR) can be attributed to the omission of appropriate monitor reaction for flux measurement, outdated nuclear spectroscopic data, and use of inadequately optimized gamma (γ) spectroscopy. Consequently, the estimation of the cross sections of Se isotopes is essential for nuclear waste management, medical radioactive isotopes, and reactor design [4, 5].

Se occurs naturally as six stable isotopes: ^{74}Se (0.86 %),

Received 3 December 2025; Accepted 9 June 2026; Accepted manuscript online 10 June 2026

† E-mail: nandlal.singh@dseu.ac.in
‡ E-mail: parginkumar@gmail.com, pargin.bangotra@nsut.ac.in

^{76}Se (9.23 %), ^{77}Se (7.60 %), ^{78}Se (23.7 %), ^{80}Se (49.8 %), and ^{82}Se (8.82 %). The residual nuclei from the (n, p) reaction channel, ^{76}As, decays via β^- at 559.086 keV with a spin-parity of 2^-; the product nuclei of the ^{78}Se(n, p)^{78}As reaction decay via β^- at the characteristic γ ray energy of 694.9 keV with an intensity of 16.7 % ($J^\pi = 2^-$). For the (n, $2n$) reaction channel, the activated nuclei of ^{81}Se^g decay via β^- at the characteristic γ-ray energy of 275.990 keV with a spin-parity of $1/2^-$ and an intensity of 0.67 %. For the residual nuclei of ^{75}Se with a half-life of 119.78 d, ε decay occurs at a characteristic γ-ray energy of 121.1155 keV and ($J^\pi = 5/2^+$). For the residual nuclei of ^{77}Ge from the (n, α) reaction channel of the target nuclei (Se), decay via β^- is observed with a spin parity of $7/2^+$ at the characteristic γ-ray energy of 211.03 keV with 30.0 % intensity (Table 1).

Multiple energy cross section measurements are essential for understanding the neutron induced reaction mechanism. However, for Se isotopes, several studies have been performed in the 13−15 MeV energy region owing to contradictory reported data. Therefore, single energy measurements in this region remain important for improving the previously reported EXFOR and evaluated nuclear library data. In this study, offline γ spectroscopy was employed to measure the cross sections of the ^{76}Se(n, p)^{76}As, ^{78}Se(n, p)^{78}As, ^{82}Se(n, $2n$)^{81}Se^g, ^{76}Se(n, $2n$)^{75}Se, and ^{80}Se(n, α)^{77}Ge reactions at the neutron energy of 14.96 ± 0.22 MeV, along with detailed covariance analysis. The measured cross section values were compared with the previously reported EXFOR database and evaluated nuclear data libraries. Furthermore, the cross sections of all measured reactions were theoretically reproduced using the TALYS 2.0 code involving different nuclear level density models (ldmodel 1−6). In addition, an optimal set of parameters and total cross section contribution from the different nuclear reaction mechanisms were identified.

II. EXPERIMENTAL DETAILS

The sample (Se) was irradiated at the Neutron and Ion Irradiation Facility (NIIF) of the Institute for Plasma Research (IPR), Gandhinagar, India. Neutrons were generated via ^{3}H(D, n)^{4}He fusion reaction, where accelerated deuterium (D^+) ions were made incident on the stationary tritium (TiT) target using an electrostatic generator. The experimental set-up consisted of three subsystems of the neutron generator: (a) Isolation transformer (350 kV), Electron Cyclotron Resonance (ECR) Ion Source, (b) Low Energy Beam Transport System (LEBTS), which included a solenoid, 90° bending magnets, quadrupole system, and beam diagnostic system, (c) Medium Energy Beam Transport System (MEBTS) consisting of a quadrupole triplet magnet, switching magnets, and TiT target [6]. The schematic of the IPR 14 MeV neutron generator is shown in Fig. 1.

Table 1. Nuclear decay data of studied reactions.

Reaction	Decay data				
	Half-life	$E\gamma$ /keV	$I\gamma$ (%)	E_{th}/keV	Decay scheme
^{76}Se(n, p)^{76}As	26.254 h (11)	559.086 (10)	40.67	2207.2	β^-
^{78}Se(n, p)^{78}As	90.7 m (2)	694.9 (1)	16.7 (22)	3471	β^-
^{82}Se(n, $2n$)^{81}Se^g	18.5 m (1)	275.990 (10)	0.67 (5)	9390.5	β^-
^{76}Se(n, $2n$)^{75}Se	119.78 d (5)	121.1155 (11)	17.20 (12)	11302.02	ε
^{80}Se(n, α)^{77}Ge	11.211 h (3)	211.03 (4)	30.0 (8)	911.6	β^-

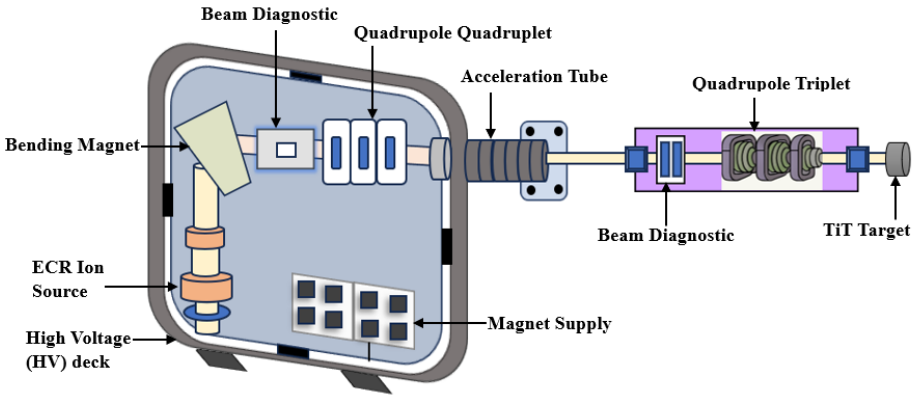

Fig. 1. (color online) Schematic of IPR 14 MeV Neutron Generator.

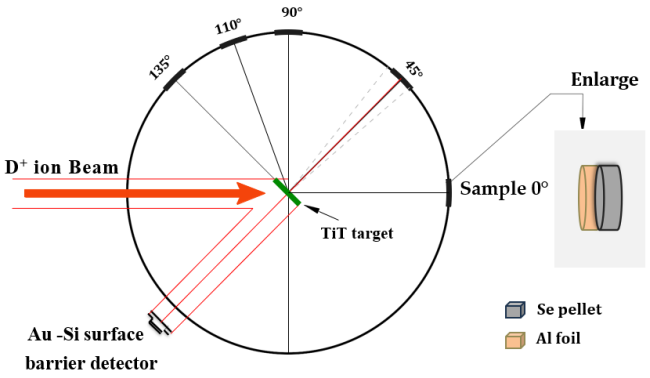

Fig. 2. (color online) Schematic of the geometric position at 0° during irradiation at IPR.

Deuterium (D^+, D^{2+}, and D^{3+}) ions were extracted from a 2.45 GHz ECR ion source. To avoid unnecessary heating of the system, the D^+ ions were separated using 90° bending magnets. Subsequently, the deuterium beam with a beam current of 2.5 mA was focused on the acceleration column with an array of quadrupole triplets in the LEBTS. Further, the beam was focused on the TiT target through the MEBTS, and 14 MeV neutrons were generated [7]. The sample was positioned at 0°, as depicted in Fig. 2. The neutron yield was estimated by Associated Alpha Diagnostic (AAD) using an Au-Si surface barrier detector placed at a 135° angle, as shown in Fig. 3. The neutron yield, flux, and irradiation details of the investigated reactions are listed in Table 2.

Circular pellets of the sample (Se) with a diameter ~1 cm were prepared by compressing Se powder (purity: 99.9 %) using a KBr hydraulic press. The Se pellet was placed behind an aluminum (Al) foil with a thickness of 0.25 mm. The pellets were wrapped in aluminum of thickness 25 μm to avoid cross-contamination. The sample details (weight, thickness, and atomic density) are presented in Table 3.

A. Calibration of Efficiency

Before counting the induced γ-ray activity inside the irradiated sample, a ^{152}Eu known standard γ-ray source was used to calibrate a High Purity Germanium (HPGe) detector. The HPGe detector has a relative efficiency of ≥ 50 % and ≤ 2.1 keV resolution at 1.33 MeV γ-ray energy of ^{60}Co. The detector was encased within a lead shield to minimize interference from background activities. The samples were positioned at a distance of 3 cm from the end cap of the HPGe detector. The counts under γ-ray

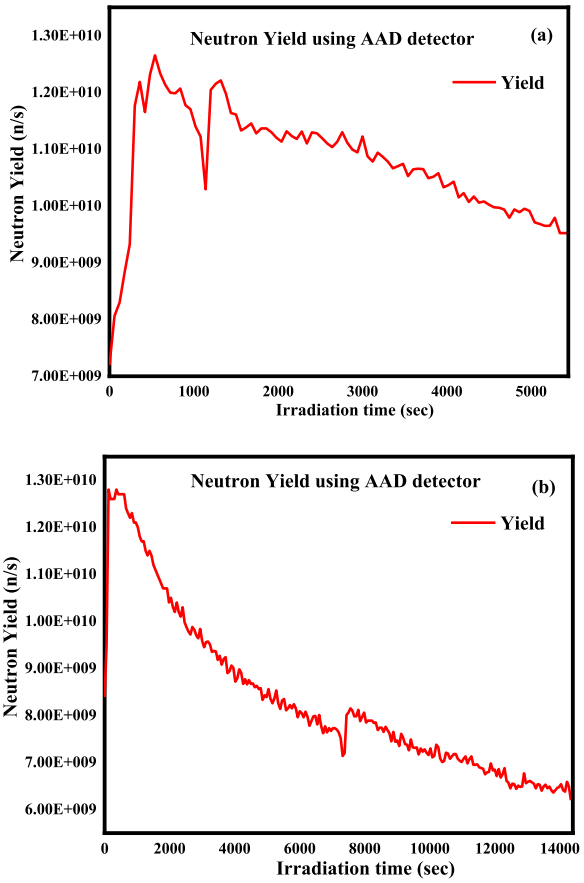

Fig. 3. (color online) Neutron yield (n/s) measured using AAD during irradiation.

photopeak were determined using GENIE software with a 16K multi-channel analyzer. The counts of the ^{152}Eu γ-ray source at the characteristic γ-ray energy are shown in Fig. 4. Furthermore, the photo-peak counts of the residual nuclei ^{76}As, ^{78}As, ^{81}Se^{g}, ^{75}Se, and ^{77}Ge at the characteristic γ-ray energies of 559.086 keV, 694.9 keV, 275.990 keV, 121.1155 keV, and 211.03 keV, respectively, are shown in Fig. 5.

III. DATA ANALYSIS

A. Estimation of neutron energy

The D-T reaction with Q value (17.58 MeV), which is initiated with the deuteron energy (E_d) and emitted kinetic energy (E_n) of the neutrons at an angle θ (0°), is determined using Eq. (1) [8].

$$[E_n(\theta)]^{\frac{1}{2}} = \frac{(M_d M_n E_d)^{\frac{1}{2}} \cos\theta + \left[M_d M_n E_d \cos^2\theta + \{M_\alpha + M_n\}(M_\alpha Q + E_d(M_\alpha - M_n))\right]^{\frac{1}{2}}}{M_\alpha + M_n}, \quad (1)$$

Table 2. Neutron yield, flux, irradiation time (s), cooling time (s), and counting time (s) of the studied reactions.

Reaction	Yield/(n/s)	Flux (e^{09})/(n/cm^2 /s)	Irradiation time	Cooling time	Counting time
^{76}Se(n, p)^{76}As	1.08e+10	1.53±0.07	5400	3765	300.74
^{78}Se(n, p)^{78}As		1.50±0.07	5400	3765	300.74
^{82}Se(n, 2n)^{81}Se^{g}		1.53±0.07	5400	975	300.52
^{76}Se(n, 2n)^{75}Se	8.35e+09	1.50±0.06	14400	93299	1635.70
^{80}Se(n, α)^{77}Ge		1.53±0.06	14400	1880	253.12

Table 3. Sample details (weight, thickness, and atomic density) of the investigated reactions along with their associated uncertainties.

Reaction	Weight/g	Thickness/cm	Atomic density (10^{21})/(atom/cm^3)
^{76}Se(n, p)^{76}As	0.5111 ± 0.0001	0.175 ± 0.001	2.766 ± 0.085
^{78}Se(n, p)^{78}As	0.5111 ± 0.0001	0.175 ± 0.001	6.837 ± 0.080
^{82}Se(n, 2n)^{81}Se^{g}	0.5111 ± 0.0001	0.175 ± 0.001	2.388 ± 0.060
^{76}Se(n, 2n)^{75}Se	0.5661 ± 0.0001	0.182 ± 0.001	2.946 ± 0.091
^{80}Se(n, α)^{77}Ge	0.5661 ± 0.0001	0.182 ± 0.001	14.810 ± 1.227

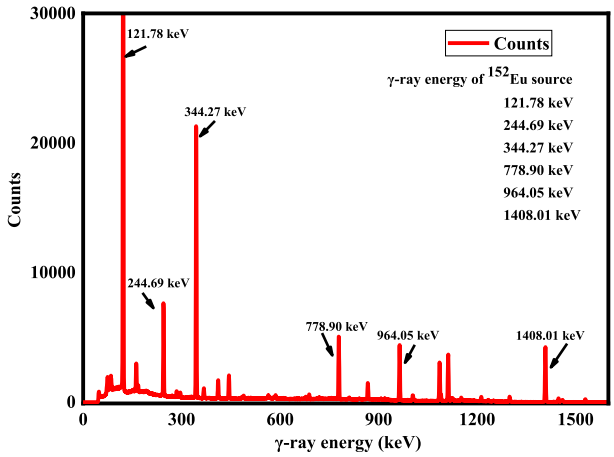

Fig. 4. (color online) Count spectra of calibrated ^{152}Eu source using GENIE software.

where M_d is the mass of deuteron, M_n is the mass of neutron, and M_α is the mass of the alpha particle. The average neutron energy at 0° emergent angle of the irradiated sample with a radius (R) at a distance (L) from the TiT target is given by Eq. (2) [9].

$$< E > = \frac{2L^2}{R^2} \int_0^{\tan^{-1}\left(\frac{R}{L}\right)} E_n(\theta) \left(\frac{\tan\theta}{\cos^2\theta}\right) \mathrm{d}\theta. \tag{2}$$

Here, L = 1 cm and R = 0.5 cm.

The average neutron energy for the irradiated sample from Eq. (2) is 14.96 MeV. The average energy of the neutrons is affected by two factors: the D^+ ion diameter (2.5 cm) and size of the sample. The uncertainty from both factors are propagated into the final neutron energy calculated using the square quadrature method. Therefore, the calculated neutron energy and its uncertainty are 14.96 ± 0.22 MeV.

B. Efficiency Calculation

Efficiency calibration of the HPGe detector was performed using a known ^{152}Eu multi γ-ray source (initial activity N_0 = 43.7 kBq, half-life = 13.51 yrs, and date of manufacture = 24 February 2009). The detector efficiency (ε) at a distance of 3 cm from the end cap for a point source is given by Eq. (3).

$$\varepsilon = \frac{k_c C}{N_0 I_\gamma t_c \mathrm{e}^{-\lambda t}} \times \epsilon_P, \tag{3}$$

where C denotes the counts under the photopeak, N_0 is the initial activity of the ^{152}Eu source, k_c is the correction factor for the coincidence summing effect calculated from EFFTRAN [10], I_γ is the intensity of the characteristic γ-ray, λ is the decay constant, t_c is the counting time (s), t is the elapsed time, and ϵ_P is the geometry efficiency of the detector, which is calculated using Eq. (4), as follows:

$$\epsilon_p = \frac{\omega}{4\pi} = \frac{2\pi\left[1 - \frac{p}{\sqrt{p^2+b^2}}\right]}{4\pi}. \tag{4}$$

ϵ_p includes the solid angle (ω), p is the distance from the source to detector, and b is the radius of the detector.

From Eq. (3), the efficiency is a function of four variables (C, I_γ, N_0, λ), and the uncertainty in the efficiency of the detector can be estimated using Eq. (5) [11], as fol-

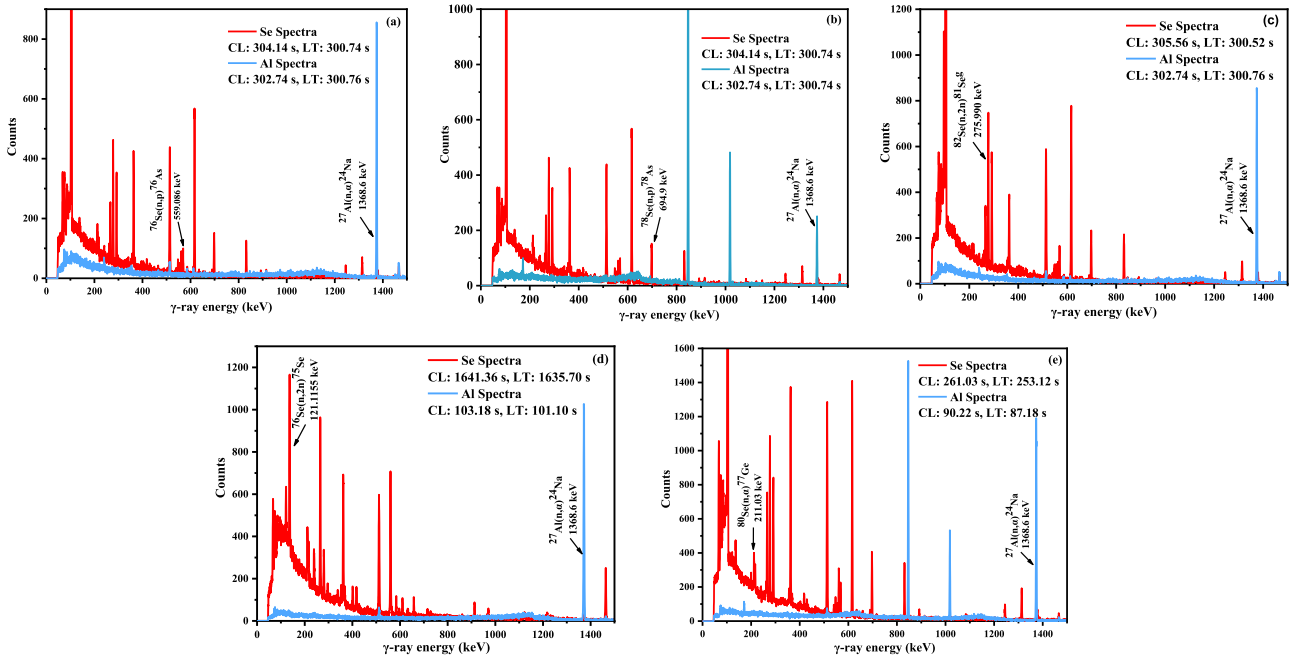

Fig. 5. (color online) Spectra of γ-ray photopeak for the residual nuclei of sample (Se) and monitor (Al).

lows:

$$\left(\frac{\Delta\varepsilon_i}{\varepsilon_i}\right) = \sqrt{\left(\frac{\Delta C_i}{C_i}\right)^2 + \left(\frac{\Delta I_{\gamma i}}{I_{\gamma i}}\right)^2 + \left(\frac{\Delta N_o}{N_o}\right)^2 + (t\Delta\lambda)^2}. \quad (5)$$

The interpolated efficiency of the detector was estimated using a linear parametric function (Eq. 6) by Geraldo *et al.* [12] as

$$\ln(\varepsilon_m) = \sum_{k=1}^{n} P_k [\ln(E_m)]^{k-1}, \quad 1 < m < 6, 1 < n < 4. \quad (6)$$

The fitted efficiency curve of the HPGe detector is depicted in Fig. 6. In the aforementioned equation, ε_m is the corresponding efficiency of the characteristic γ-ray (E_m), and P_k denotes the fitting parameters given by Eq. (7).

$$\hat{P} = \left(A^T V_z^{-1} Z\right) V_{\hat{P}}. \quad (7)$$

Here, $V_{\hat{P}}$ is the covariance matrix, and matrix V_Z is obtained from Eq. (8), as follows:

$$V_Z = \frac{(V_\varepsilon)_{ij}}{\varepsilon_i \varepsilon_j}. \quad (8)$$

The goodness of fit (value of n) is given by the chi-square, as shown in Eq. (9) [13−14].

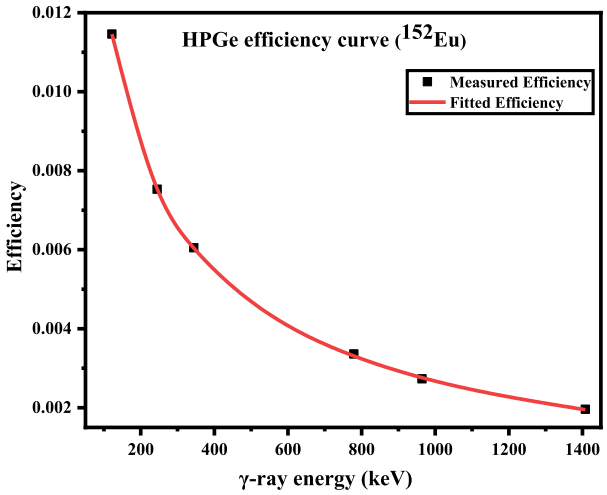

Fig. 6. (color online) Fitted efficiency curve of ^{152}Eu γ-ray source.

$$\chi^2 = (Z - AP)' V_Z^{-1} (Z - AP). \quad (9)$$

The inferred fitted parameters ($\hat{P}$) are −5.923, −0.879, −0.126, and −0.017; the chi- square value is 5.21, and $\frac{\chi^2}{6-4} \approx 2.6$. The interpolated efficiencies of the residual nuclei ^{76}As, ^{78}As, ^{81}Se^{g}, ^{75}Se, and ^{77}Ge at the characteristic γ-ray are mentioned in Table 4.

C. Assessment of reactions cross section

The cross sections of the Se isotopes were estimated using the ratio method (Eq. (10)) with ^{27}Al(n, α)^{24}Na as

Table 4. Efficiency, uncertainty, covariance, and correlation matrix of studied reactions.

Reaction	Efficiency (e^{-03})	Uncertainty (e^{-03})	Covariance Matrix (e^{-10})					Correlation Matrix				
^{76}Se(n, p)^{76}As	4.29	0.023	5.37					1				
^{78}Se(n, p)^{78}As	3.63	0.029	6.75	8.86				0.97	1			
^{82}Se(n, 2n)^{81}Se^{g}	6.98	0.066	10.08	10.11	44.63			0.65	0.50	1		
^{76}Se(n, 2n)^{75}Se	11.50	0.027	2.34	3.15	7.18	7.48		0.36	0.38	0.39	1	
^{80}Se(n, α)^{77}Ge	8.26	0.034	3.88	3.54	22.21	4.65	11.78	0.48	0.34	0.96	0.49	1

the reference monitor reaction [15, 16].

$$\sigma_r = \sigma_m \frac{[NI_\gamma \varepsilon f]_m [C\lambda \frac{CL}{LT}]_r}{[NI_\gamma \varepsilon f]_r [C\lambda \frac{CL}{LT}]_m} \prod_k \frac{(C_k)_r}{(C_k)_m}, \tag{10}$$

where the subscripts r and m denote the studied reactions and monitor reaction, respectively.

The reference monitor reaction cross section (σ_m) of ^{27}Al(n, α)^{24}Na is 108.6 ± 1.38 mb, taken from the IRDFF-II evaluated data library [17] at the bounding energy points (14.8 and 15.0 MeV) for 14.96 MeV neutron energy by using the linear interpolation method.

In the aforementioned Eq. (10), N denotes the number of nuclei (includes the atomic mass (AM), isotopic abundance (a), weight of the sample (W)), I_γ is the intensity of γ-ray abundance, ε is the efficiency at the characteristic γ ray energy (E_γ), f is the time factor, C denotes the count under the photo-peak, λ is the decay constant, CL is the real time (clock time), LT denotes the live time, and C_k denotes the correction factors.

$$f = \left(1 - e^{-\lambda T}\right)\left(e^{-\lambda t_1}\right)\left(1 - e^{-\lambda t_2}\right), \tag{11}$$

In Eq. (11), f is a time factor that includes the irradiation time (T), cooling time (t_1), and counting time (t_2) in seconds.

Moreover, the correction factor (C_k) mentioned in Eq. (10) is defined as follows:

γ-ray self-attenuation correction factor (f_{s-att}):

$$f_{s-att} = \frac{\mu t d}{1 - e^{-\mu t d}}, \tag{12}$$

where μ is the mass attenuation coefficient (cm^2 g^{-1}) at the characteristic γ-ray energy taken from XMuDat [18], t is the thickness of the sample (cm), and d is the density of the sample (g cm^{-3}) in Eq. (12).

Geometry correction factor (f_g):

$$f_g = \frac{(h + \frac{t}{2})^2}{h^2}, \tag{13}$$

where h is the distance from the surface of the sample to the detector (cm); t is the thickness of the sample (cm) in Eq. (13).

Neutron fluctuation correction factor (f_{flue}):

$$f_{\text{flue}} = \frac{\sum_i^p \varphi_i \left(1 - e^{-\lambda \Delta t_i}\right) e^{-\lambda T_i}}{\varphi S}. \tag{14}$$

In the aforementioned Eq. (14), p denotes the time intervals into which the irradiation time (T) is divided; Δt_i represents the duration of the i^{th} time interval; T_i is the time elapsed from the end of the i^{th} interval to the completion of irradiation; φ_i denotes the average neutron flux over the sample throughout Δt_i; and S is the growth factor of the residual nuclei ($S = 1 - \exp(-\lambda T)$) [19–20].

The calculated correction factors of the studied reactions are shown in Table 5.

The uncertainty in the measured cross section values is evaluated using the quadratic sum formula shown in Eq. (15) [10].

$$\left(\frac{\Delta\sigma_r}{\sigma_r}\right)^2 = \sum_a \left(\frac{\Delta a_r}{a_r}\right)^2 + \sum_a \left(\frac{\Delta a_m}{a_m}\right)^2 + \sum_a \left(\frac{\Delta\sigma_m}{\sigma_m}\right)^2,$$
$$a = a\left(C, N, \varepsilon, I_\gamma, f, C_k\right). \tag{15}$$

D. Contribution from the other reaction channel

The contribution of the competing reaction channel may be from the same residual nuclei yield from the parent nuclei and identical characteristic γ-ray emission from different residual nuclei. In this study, the residual nuclei ^{81}Se^{g} emits the identical characteristic γ-ray energy from its metastable state (^{81}Se^{m}) [21]. Therefore, the contribution of the competing reaction is reduced using Eq. (16).

$$R = \frac{C_{obs_{r1}}}{C_{obs_{r2}}} = \frac{a_{r1}\sigma_{r1}\tau_{1/2_{r1}}}{a_{r2}\sigma_{r2}\tau_{1/2_{r2}}}. \tag{16}$$

In Eq. (16), r_1 and r_2 are the reactions, a is the isotopic abundance, σ is the cross section taken from the TENDL-

Table 5. List of correction factors for the studied reactions.

Correction factors	^{76}Se(n, p)^{76}As	^{78}Se(n, p)^{78}As	^{82}Se(n, 2n)^{81}Se^{g}	^{76}Se(n, 2n)^{75}Se	^{80}Se(n, α)^{77}Ge
f_{s-att}	1.03	1.02	1.05	1.19	1.07
f_g	1.06	1.06	1.06	1.06	1.06
f_{flue}	1.29	1.28	1.29	0.99	0.98

2025 library, and $\tau_{1/2}$ is the half- life (s).

Specifically, r_1 is the ^{82}Se(n, 2n)^{81}Se^{g} reaction, and r_2 is the ^{82}Se(n, 2n)^{81}Se^{m} reaction. σ_{r1} is 471.33 mb and σ_{r2} is 874.88 mb. $\tau_{1/2_{r1}}$ is 1107 s and $\tau_{1/2_{r2}}$ is 3436.8 s.

The ratios of the cross-section of the ground state to that of the isomeric state for the reaction ^{82}Se(n, 2n)^{81}Se are approximately equal for both the evaluated nuclear data libraries (JEFF-4.0 and TENDL-2025). This indicates a negligible effect of the choice of the evaluated nuclear data library on the final cross section value. However, TENDL-2025 was selected, as it is a TALYS-based evaluated nuclear data library incorporating both default and adjusted parameters and other codes wrapped into a Total Monte Carlo loop for uncertainty quantification. Hence, it provides theoretically consistent predictions for the separation of the contribution of the metastable state from that of the ground state.

IV. COVARIANCE ANALYSIS

Covariance analysis is a statistical approach implemented to describe and evaluate the degree of correlation between various parameters of the studied reactions. The covariance (correlations) between the parameters must be considered to neglect the underestimation or overestimation of the uncertainty in the value of the cross section. Consequently, the uncertainty associated with different parameters were considered to evaluate the uncertainties in the cross sections and covariance matrices of the Se reactions. Moreover, the correlation coefficient between any two parameters is represented in three ways: if two parameters (x_1 and x_2) are independent of each other, they are uncorrelated (Cor (x_1, x_2) = 0); if the parameters are governed by comparable common factors, they are correlated (Cor (x_1, x_2) = 1); and if the parameters are partially related to each other, they are considered to be partially correlated (0 < Cor (x_1, x_2) < 1) [11]. The correlations between the various studied Se reactions ("cross- correlation") were estimated, as shown in Table 6.

The efficiencies are partially correlated with each other, as they are derived from the common calibrated curve (Fig. 6). Therefore, the correlation coefficients corresponding to the efficiencies are calculated by Eq. (17).

$$\text{Corr}\left(\varepsilon_i, \varepsilon_j\right) = \frac{\text{Cov}\left(\varepsilon_i, \varepsilon_j\right)}{\sqrt{\text{var}\left(\varepsilon_i\right)}\sqrt{\text{var}\left(\varepsilon_j\right)}}, \tag{17}$$

Table 6. Correlation coefficient of the studied reactions with respect to the various parameters.

Attributes	Cor (p, q)	Cor (p, r)	Cor (p, s)	Cor (p, t)	Cor (q, r)	Cor (q, s)	Cor (q, t)	Cor (r, s)	Cor (r, t)	Cor (s, t)
σ_m	1	1	1	1	1	1	1	1	1	1
C_m	0	1	0	0	0	0	0	0	0	0
C_r	0	0	0	0	0	0	0	0	0	0
λ_m	1	1	1	1	1	1	1	1	1	1
λ_r	0	0	0	0	0	0	0	0	0	0
$I_{\gamma m}$	1	1	1	1	1	1	1	1	1	1
$I_{\gamma r}$	0	0	0	0	0	0	0	0	0	0
AM_m	1	1	1	1	1	1	1	1	1	1
AM_r	0	0	1	0	0	0	0	0	0	0
W_m	1	1	0	0	1	0	0	0	0	1
W_r	1	1	0	0	1	0	0	0	0	1
a_m	1	1	1	1	1	1	1	1	1	1
ε_m	1	1	1	1	1	1	1	1	1	1
ε_r	0.97	0.65	0.36	0.48	0.50	0.38	0.34	0.39	0.96	0.49
f_{s-att_m}	1	1	0	0	1	0	0	0	0	1
f_{s-att_r}	0	0	0	0	0	0	0	0	0	0
f_{g_m}	1	1	1	1	1	1	1	1	1	1
f_{g_r}	1	1	0	0	1	0	0	0	0	1

* p = ^{76}Se(n, p)^{76}As, q = ^{78}Se(n, p)^{78}As, r = ^{82}Se(n, 2n)^{81}Se^{g}, s = ^{76}Se(n, 2n)^{75}Se, and t = ^{80}Se(n, α)^{77}Ge.

where $\text{Cov}(\varepsilon_i, \varepsilon_j)$ is the covariance matrix presented in Table 4.

The partial uncertainty matrices and micro-correlation matrices are used to construct the covariance matrix for the investigated reactions using the below expression (Eq. 18) [13].

$$(V_\sigma)_{ij} = \sum_m e_{im} S_{ijm} e_{jm}. \tag{18}$$

where e_{im} and e_{jm} are the partial uncertainty matrices for the i^{th} and j^{th} parameters, and S_{ijm} is the micro-correlation matrix for the various parameters. All parameters with their uncertainties are used to construct the covariance matrix. The calculated cross section with fractional uncertainty, covariance, and correlation matrix for the ^{76}Se(n, p)^{76}As, ^{78}Se(n, p)^{78}As, ^{82}Se(n, 2n)^{81}Se^{g}, ^{76}Se(n,

Table 7. Measured cross section, uncertainty, covariance, and correlation matrix of the studied reactions.

Reaction	σ /mb	$\Delta\sigma$ /mb	Covariance Matrix					Correlation Matrix				
^{76}Se(n, p)^{76}As	55.30	4.09	16.71					1				
^{78}Se(n, p)^{78}As	18.77	1.12	2.19	1.18				0.49	1			
^{82}Se(n, 2n)^{81}Se^{g}	529.78	51.23	65.13	20.97	2613.05			0.31	0.37	1		
^{76}Se(n, 2n)^{75}Se	903.98	55.99	102.15	33.63	980.59	3134.89		0.44	0.55	0.34	1	
^{80}Se(n, α)^{77}Ge	2.01	0.12	0.22	0.07	2.21	3.77	0.01	0.46	0.57	0.36	0.56	1

2n)^{75}Se, and ^{80}Se(n, α)^{77}Ge reactions are depicted in Table 7.

V. RESULTS AND DISCUSSION

A. Experimentally measured cross sections of reactions

1. *^{76}Se(n, p)^{76}As reaction*

The measured cross section of the ^{76}Se(n, p)^{76}As reaction leading to the residual nucleus of ^{76}As is 55.30 ± 4.09 mb with a fractional uncertainty of 7.40 % at the neutron energy of 14.96 ± 0.22 MeV (Table 7). The measured cross section exceeds the value reported by T. S. Ganesapandy *et al.* by 15 % [22] at the neutron energy of 14.77 MeV. This difference is attributed to the use of a powder as the target material, which resulted in the geometry correction factor being neglected in the measurement of the reaction cross section (Fig. 7). The cross section reported by A. A. Filatenkov *et al.* [23] is 54.4 mb at the neutron energy of 14.8 MeV with ^{93}Nb(n, 2n)^{92}Nb^{m} as the monitor reaction. Moreover, the cross section reported by A. A. Filatenkov *et al.* does not incorporate the geometry correction factor. However, the error bar of the measured cross section values is consistent with the JEFF-4.0 evaluated data library [24]. The measured cross section of the ^{76}Se(n, p)^{76}As reaction deviated by 2.80 % from the results of the CENDL-3.2 nuclear data library, as shown in Table 8 [25].

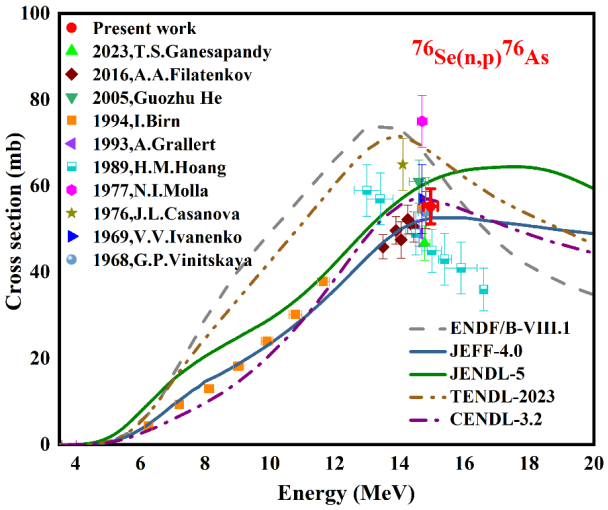

Fig. 7. (color online) Comparison between the measured, previously reported, ENDF/B-VIII.1, JEFF-4.0, JENDL-5, TENDL-2023, and CENDL-3.2 library cross section data for the ^{76}Se(n, p)^{76}As reaction.

2. *^{78}Se(n, p)^{78}As reaction*

The measured cross section of the ^{78}Se(n, p)^{78}As reaction leading to the residual nuclei of ^{78}As is 18.77 ± 1.12 mb, associated with an uncertainty of 5.98 % at the neutron energy of 14.96 MeV. The measured cross section is consistent with the previously reported data. However, the cross section uncertainty (13.1 %) reported by T. S. Ganesapandy *et al.* [22] is significantly higher than the measured cross section uncertainty (5.98 %). The cross section reported by A. A. Filatenkov *et al.* is 21.2 ± 2.3

Table 8. Percentage deviation (%) of the measured cross section from the data in various evaluated libraries for the studied reactions.

Reaction	Percentage Deviation of cross section				
	ENDF/B-VIII.1	JEFF-4.0	JENDL-5	TENDL-2023	CENDL-3.2
^{76}Se(n, p)^{76}As	18.97	−5.05	11.25	22.68	2.80
^{78}Se(n, p)^{78}As	11.51	7.25	11.51	90.41	−3.46
^{82}Se(n, 2n)^{81}Se^{g}	-	−11.07	-	−38.97	-
^{76}Se(n, 2n)^{75}Se	5.09	7.15	4.56	−16.86	−10.99
^{80}Se(n, α)^{77}Ge	929.80	59.91	9.98	135.27	159.05

mb at the neutron energy of 14.81 MeV [23], surpassing the measured cross section value in this study by approximately 11.4 % (Fig. 8). Moreover, the measured cross section lies within the uncertainty range and shows deviations of 7.25 % and −3.46 % from the JEFF-4.0 [24] and CENDL-3.2 [25] evaluated nuclear data libraries, respectively (Table 8).

3. $^{82}Se(n, 2n)^{81}Se^{g}$ reaction

The measured cross section of the ^{82}Se(n, $2n$)^{81}Se^{g} reaction is 529.78 ± 51.23 mb with a fractional uncertainty of 9.67 % (Fig. 9). The measured cross section is significantly higher than the previously reported data. A. A. Filatenkov *et al.* [23] reported the cross section at the neutron energy of 14.84 MeV, corresponding to the characteristics γ-ray energy of 290.0 keV with an uncertainty of 26.3 %. Moreover, the ground state cross section reported by Junhua Luo *et al.* [26] using the characteristic γ-ray energy of 275.93 keV was 22.9 % lower than the measured value. This difference is attributed to the subtraction of the contribution arising from the metastable state (^{81}Se^{m}) corresponding to 103.01 keV and ^{93}Nb(n, $2n$)^{92}Nb^{m} as the monitor reaction. Furthermore, the measured cross section is within the uncertainty range of the JEFF-4.0 library (Fig. 9).

4. $^{76}Se(n, 2n)^{75}Se$ reaction

The measured cross section of the ^{76}Se(n, $2n$)^{75}Se reaction leading to the residual nuclei ^{75}Se is 903.98 ± 55.99 mb with an uncertainty of 6.19 % (Fig. 10). The measured cross section is consistent with the latest reported data of T. S. Ganesapandy *et al.* [22] at the neutron energy of 14.77 MeV. At the neutron energy of 15 MeV, the cross section reported by H. M. Hoang *et al.* [27] exhibits a slightly higher uncertainty than that of the measured cross section. Moreover, the measured cross section is slightly above the excitation curve of the TENDL-2023 evaluated data library [28]. Furthermore, the measured cross section shows better agreement with the CENDL-3.2 nuclear data library, as depicted in Fig. 10.

5. $^{80}Se(n, \alpha)^{77}Ge$ reaction

The measured cross section of the ^{80} Se(n, α)^{77}Ge reaction is 2.01 ± 0.12 mb with an uncertainty of 5.96 % (Fig. 11). Experimental studies have not been conducted for over two decades within the neutron energy region of 14.9 MeV. Therefore, the measurement in this study was compared with the neighboring neutron energies. In the EXFOR data, a large discrepancy was found in the reaction cross section uncertainty, which varied from 8% to 34%. At the neutron energy of 15 MeV, the cross section reported by Guozhu He *et al.* [29] was estimated using the ^{56}Fe(n, p)^{56}Mn monitor reaction with

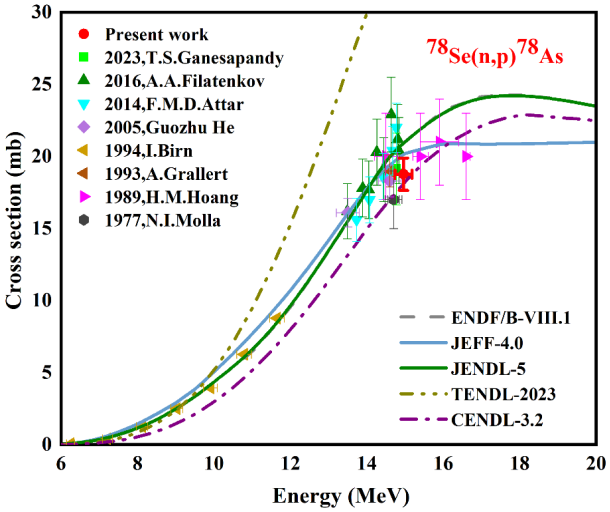

Fig. 8. (color online) Comparison of the data of this study with the previously reported, ENDF/B-VIII.1, JEFF-4.0, JENDL-5, TENDL-2023, and CENDL-3.2 library cross section data for the ^{78}Se(n, p)^{78}As reaction.

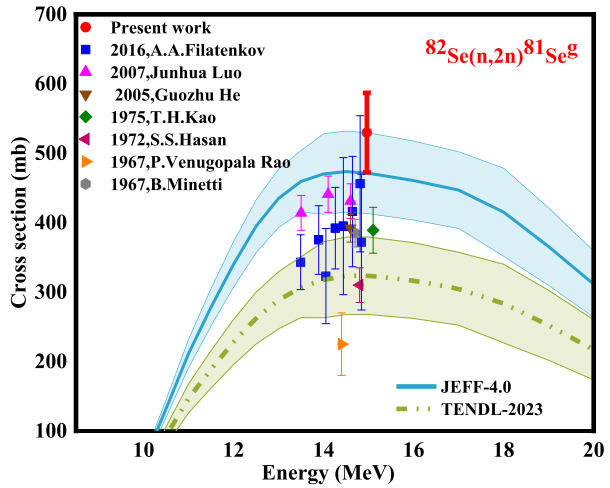

Fig. 9. (color online) Comparison of the present, previous reported, JEFF-4.0, and TENDL-2023 library cross section data of the ^{82}Se(n, $2n$)^{81}Se^{g} reaction.

an uncertainty of 14.3 %. Furthermore, the measured cross section is consistent with the JENDL-5 library (2.25 mb) [30].

B. Theoretically simulated cross section using TALYS code

A comprehensive theoretical analysis was performed to reproduce the cross section using the TALYS-2.0 code by employing different nuclear level density (NLD) models (Table 9) and a combination of other relevant parameters. For a quantitative evaluation of the measured and theoretically reproduced cross sections using various level density models (ldmodel) and adjusted parameters, the chi-square (χ^2) was calculated using Eq. (19) by J.

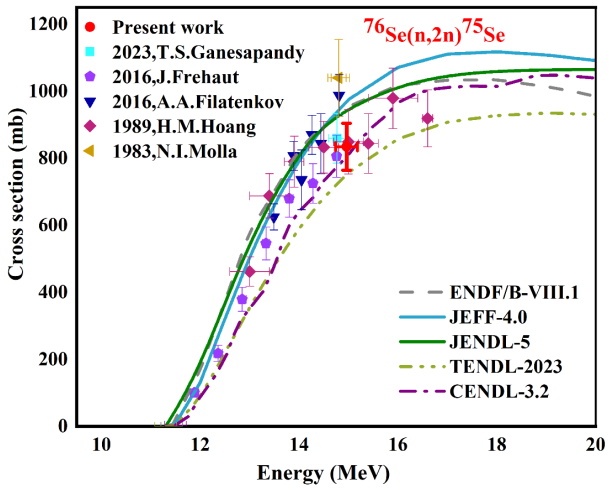

Fig. 10. (color online) Comparison of the data of this study with the previously reported data and ENDF/B-VIII.1, JEFF-4.0, JENDL-5, TENDL-2023, and CENDL-3.2 library cross section data for the ^{76}Se(n, $2n$)^{75}Se reaction.

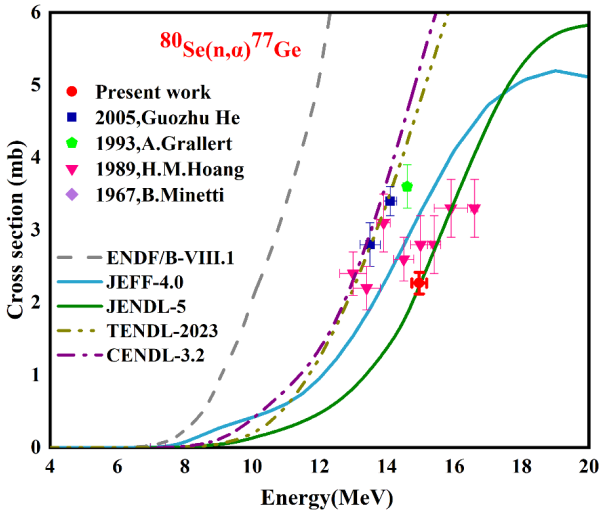

Fig. 11. (color online) Comparison of the data of this study with the previously reported data and ENDF/B-VIII.1, JEFF-4.0, JENDL-5, TENDL-2023, and CENDL-3.2 library cross section data for the ^{80}Se(n, α)^{77}Ge reaction.

Luo et al. for each reaction, as shown in (Tables 10, 11) [31].

$$\chi^2 = \frac{\sum_{i=1}^{N}[(\sigma_i^{\mathrm{Cal}} - \sigma_i^{\mathrm{exp}})/(k\Delta\sigma_i^{\mathrm{exp}})]^2}{N}, \qquad (19)$$

where σ_i^{Cal} denotes the theoretical calculated cross section, σ_i^{exp} is the experimentally measured cross section, $\Delta\sigma_i^{\mathrm{exp}}$ is the error (uncertainty) in the experimentally measured cross section, k is the coverage factor (k = 2), and N is the number of experimental data including those measured in this study and those in the EXFOR database. N takes the values 8, 7, 7, 6, and 5 for the ^{76}Se(n, p)^{76}As, ^{78}Se(n, p)^{78}As, ^{82}Se(n, $2n$)^{81}Se^{g}, ^{76}Se(n, $2n$)^{75}Se, and ^{80}Se(n, α)^{77}Ge reactions, respectively.

In this study, the cross sections of the ^{76}Se(n, p)^{76}As, ^{78}Se(n, p)^{78}As, ^{82}Se(n, $2n$)^{81}Se^{g}, ^{76}Se(n, $2n$)^{75}Se, and ^{80}Se(n, α)^{77}Ge reactions were additionally reproduced

Table 9. Cross sections (mb) of the reactions using different level density models of TALYS 2.0.

Reaction	Level density models					
	ldmodel 1	ldmodel 2	ldmodel 3	ldmodel 4	ldmodel 5	ldmodel 6
^{76}Se(n, p)^{76}As	38.00	52.21	**53.90**	52.57	41.85	44.63
^{78}Se(n, p)^{78}As	26.36	24.10	26.88	35.71	**21.70**	22.48
^{82}Se(n, $2n$)^{81}Se^{g}	**515.49**	473.24	447.48	457.55	488.96	467.27
^{76}Se(n, $2n$)^{75}Se	971.89	854.55	763.79	**855.55**	946.51	626.46
^{80}Se(n, α)^{77}Ge	0.96	3.15	1.32	1.47	**1.99**	1.32

Table 10. Chi square (χ^2) for the calculated cross section using level density models of the studied reactions.

Reaction	χ^2 (k = 2, confidence level = 95 %)					
	ldmodel 1	ldmodel 2	ldmodel 3	ldmodel 4	ldmodel 5	ldmodel 6
^{76}Se(n, p)^{76}As	3.37	0.71	**0.65**	0.69	2.25	1.63
^{78}Se(n, p)^{78}As	5.32	2.64	6.08	26.82	**0.86**	1.31
^{82}Se(n, $2n$)^{81}Se^{g}	**6.30**	3.22	1.94	2.39	4.22	2.88
^{76}Se(n, $2n$)^{75}Se	0.53	0.35	1.15	**0.35**	0.37	3.91
^{80}Se(n, α)^{77}Ge	9.05	4.77	5.48	4.33	**1.84**	5.48

Table 11. Total cross section (σ) and contributions of the reaction mechanism using the adjusted parameters of TALYS 2.0 code.

Reaction	Adjusted parameters					Theoretical calculated cross section *σ/mb				
	level density model	optical potential model	pre-equilibrium model	γ ray SFM	WFM	*σ/mb	χ^2	Direct/mb	pre-equilibrium/mb	Compound nucleus/mb
^{76}Se(n, p)^{76}As	ldmodel 2	jlmomp	preeqmode 3	strength 9	widthmode 1	54.23	0.65	0.00	12.94	41.29
^{78}Se(n, p)^{78}As	ldmodel 2	dispersion	preeqmode 3	strength 9	widthmode 1	17.27	0.47	0.86	4.53	13.61
^{82}Se(n, $2n$)^{81}Se^{g}	ldmodel 1	localomp y	preeqmode 3	strength 1	widthmode 1	537.22	8.36	0.00	0.00	537.22
^{76}Se(n, $2n$)^{75}Se	ldmodel 2	localomp y	preeqmode 3	strength 2	widthmode 1	926.30	0.30	0.00	0.00	926.30
^{80}Se(n, α)^{77}Ge	ldmodel 5	localomp y	preeqmode 1	strength 9	widthmode 1	1.97	4.45	0.13	0.66	1.43

*σ (mb) = cross section (mb).

with a set of adjusted parameters, as shown in Table 11 [32−34]. Furthermore, the contributions of various reaction mechanisms, namely, compound nucleus, pre-equilibrium, and direct, to the total cross section of the aforementioned reactions were examined (Table 11).

1. *Estimation of cross section using Nuclear Level Density (NLD) models*

The measured cross sections of the ^{76}Se(n, p)^{76}As, and ^{78}Se(n, p)^{78}As, ^{82}Se(n, $2n$)^{81}Se^{g}, ^{76}Se(n, $2n$)^{75}Se, and ^{80}Se(n, α)^{77}Ge reactions were compared with those of all six nuclear level density models of TALYS code. For the ^{76}Se(n, p)^{76}As reaction, the cross section reproduced through ldmodel 3 (Generalized Superfluid model) [35−38] with the default optical model, pre-equilibrium, width fluctuation correction model, and γ strength function model [39] shows better agreement with the measured cross section, as depicted in Fig. 12 (a). Moreover, the measured cross section (55.30 mb) exceeds the value calculated using ldmodel 3 (53.90 mb) by approximately 2.5 %. Furthermore, the cross sections estimated with ldmodel 2 (Back-Shifted Fermi Gas model) [40] and ldmodel 4 (S. Goriely microscopic model) [41] lie in the error bar of the measured cross section.

For the ^{78}Se(n, p)^{78}As reaction, the cross section simulated from the nuclear level density models for the ^{78}Se(n, p)^{78}As reaction varies from 21.70 to 35.71 mb (Fig. 12 (b)). The cross section obtained via ldmodel 5 (S. Hilarie microscopic model) is the nearest to the measured value [42]. However, the theoretical cross sections obtained using the other microscopic level density models, *i.e.*, ldmodel 4 and ldmodel 6, exceed the measured cross section by approximately 46 % and 15 %, respectively.

The theoretical reproduced cross sections of the ^{82}Se(n, $2n$)^{81}Se^{g} reaction using ldmodel 1, ldmodel 2, ldmodel 3, ldmodel 4, ldmodel 5, and ldmodel 6 are 515.49, 473.24, 447.48, 457.55, 488.96, and 467.27 mb, respectively (Fig. 13 (a)). In comparison with the other NLD models, Constant Temperature nuclear level density model (ldmodel 1) of TALYS reproduces a better cross section value for the ^{82}Se(n, $2n$)^{81}Se^{g} reaction.

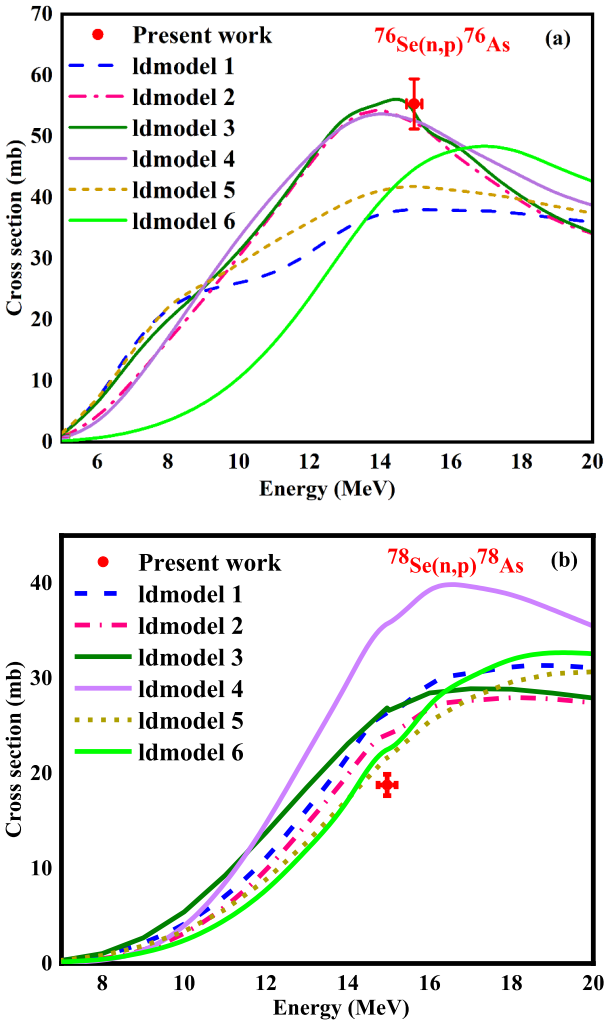

Fig. 12. (color online) Comparison of the measured cross section and theoretically reproduced cross section value using various nuclear level density models for ^{76}Se(n, p)^{76}As and ^{78}Se(n, p)^{78}As reactions.

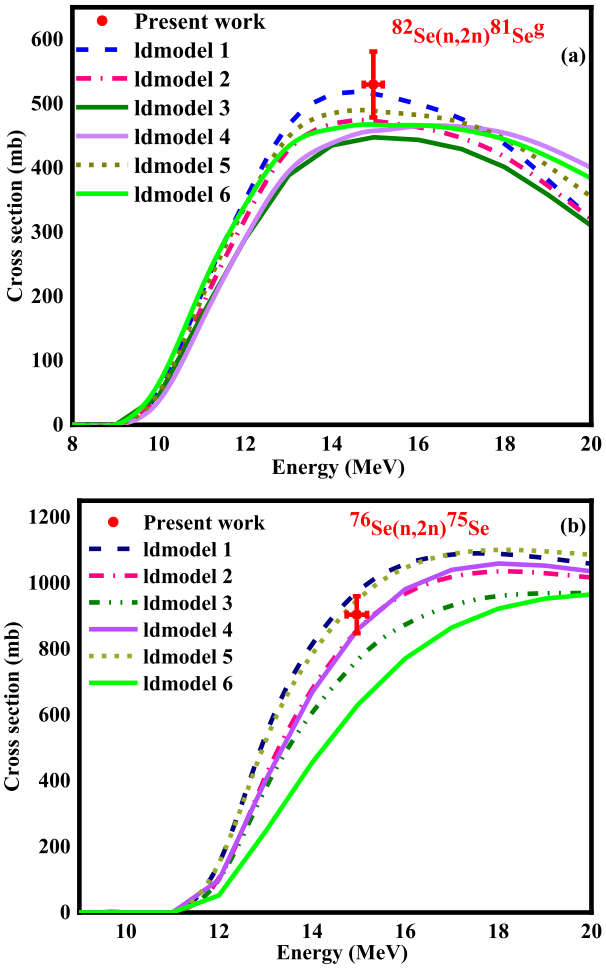

Fig. 13. (color online) Comparison of the measured and theoretically reproduced cross sections using various nuclear level density models for the ^{82}Se(n, $2n$)^{81}Se^{g} and ^{76}Se(n, $2n$)^{75}Se reactions.

For the ^{76}Se(n, $2n$)^{75}Se reaction, the cross sections obtained from ldmodel 1, ldmodel 2, ldmodel 3, ldmodel 4, ldmodel 5, and ldmodel 6 are 971.89, 854.55, 763.79, 855.55, 946.51, and 626.46 mb, respectively (Fig 13 (b)). The cross sections of the ^{76}Se(n, $2n$)^{75}Se reaction using ldmodel 2 (854.55 mb) and ldmodel 4 (855.55 mb) exceed the measured value by approximately 5.46 % and 5.35 %, respectively. Among all the NLD models, the Hartree-Fock- Bogoliubov (ldmodel 6) microscopic model shows the minimum cross section for the ^{76}Se(n, $2n$)^{75}Se reaction (Fig. 13 (b)).

The theoretical estimated cross sections of the ^{80}Se(n, α)^{77}Ge reaction, reproduced from ldmodel 1, ldmodel 2, ldmodel 3, ldmodel 4, ldmodel 5, and ldmodel 6, are 0.96, 3.15, 1.32, 1.47, 1.99, and 1.32 mb, respectively. The cross section using ldmodel 5 (S. Hilarie microscopic) level density model with other default parameters exhibits better consistency with the measured cross section, as revealed in Fig. 14. The measured cross section exceeds the theoretically obtained cross section using ldmodel 5 by approximately 0.99 %. However, ldmodel 3 and ldmodel 6 reproduce similar trends of the cross section up to 18 MeV neutron energy for the ^{80}Se(n, α)^{77}Ge reaction.

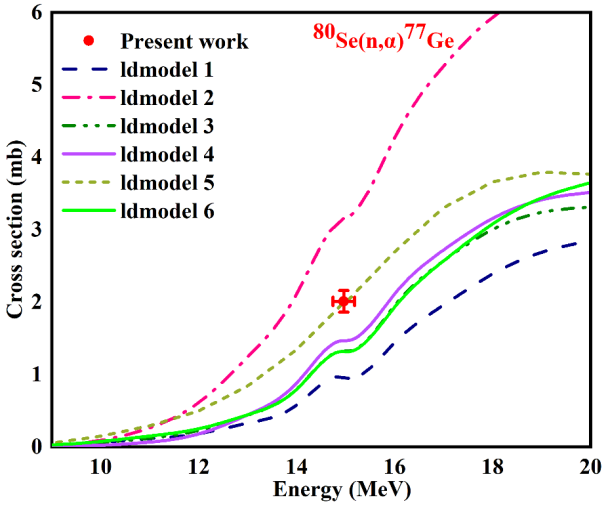

Fig. 14. (color online) Comparison of the measured cross section and theoretically reproduced cross section using various nuclear level density models for the ^{80}Se(n, α)^{77}Ge reaction.

As can be interpreted from Table 10, the selection of the best fit level density model for each reaction is validated by the smallest chi-square (χ^2) value calculated using Eq. (19). However, in the case of the ^{82}Se(n, $2n$)^{81}Se^{g} reaction, the χ^2 value is observed to be the lowest for ldmodel 3, rather than for ldmodel 1, despite predicting a better agreement with the measured result. This could be attributed to the fact that ldmodel 3 was successfully validated on EXFOR in all previous studies [23, 26]. Despite this, the present cross section is well validated by ldmodel 3 rather than ldmodel 1, as it is higher than the values in previous studies.

2. *Estimated cross section through adjusted parameters of TALYS code*

For the ^{76}Se(n, p)^{76}As reaction, the adjusted set of parameters (ldmodel 2, jlmomp, preeqmode 3, strength 9, and widthmode 1) reproduced the cross section of 54.23 mb at the neutron energy of 14.96 MeV. The cross section obtained using the adjusted parameters for the ^{76}Se(n, p)^{76}As reaction is in close agreement with the measured value in this study (55.30 mb), as depicted in Fig. 15. The Back Shifted Fermi Gas model ("ldmodel 2") provides a realistic excitation energy dependence of the level density for the residual nucleus. Moreover, the JLM optical model has been optimized and validated for the spherical and quasi-spherical nuclei by using JLM implementation. Furthermore, the inclusion of "preeqmode 3" enhances

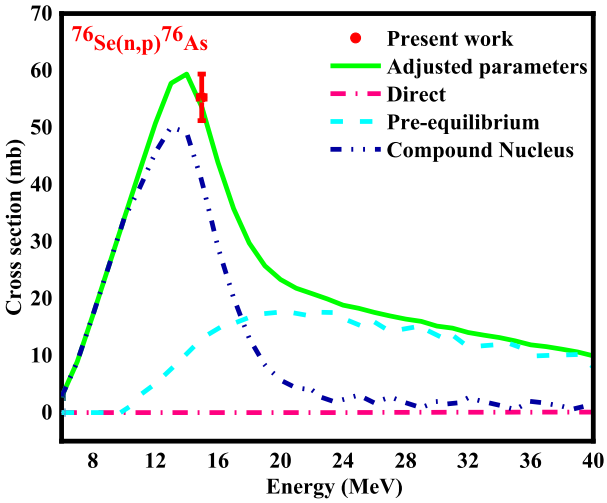

Fig. 15. (color online) Comparison of the measured cross section using the adjusted parameters of TALYS and contribution to the cross section from various reaction mechanisms for the ^{76}Se(n, p)^{76}As reaction.

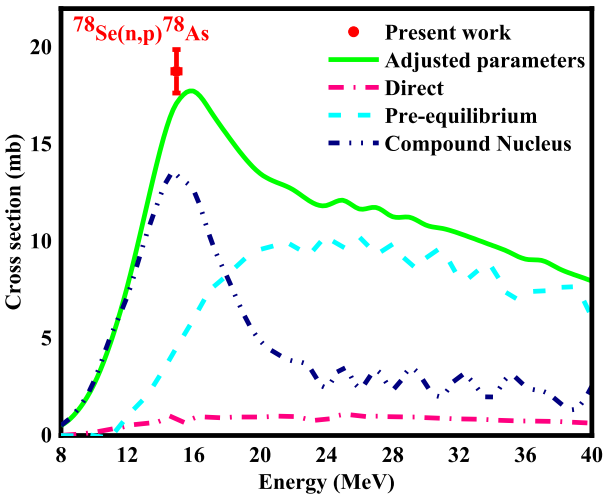

Fig. 16. (color online) Comparison of measured cross section using the adjusted parameters of TALYS and contributions to the cross section from various reaction mechanisms for the ^{78}Se(n, p)^{78}As reaction.

the exciton based multistep pre-equilibrium emission. Therefore, the aforementioned parameters are adopted as an adjusted set of parameters to reproduce the ^{76}Se(n, p)^{76}As reaction cross section. At 14.96 MeV, the reaction is predominantly governed by a compound nucleus mechanism contributing 76.13 % of the total cross section, whereas the remaining 23.87 % arises from the pre-equilibrium mechanism (Table 11). The contribution of the pre-equilibrium mechanism increases with the elevation in the neutron energy. However, the compound nucleus mechanism decreases at higher energies. The calculated excitation curve for the ^{76}Se(n, p)^{76}As reaction shows a dominant contribution of the compound nucleus reaction mechanism in a low-energy range (< 12 MeV). However, the contribution of the pre-equilibrium reaction mechanism increases from the mid-range neutron energy (~15 MeV), and a negligible contribution can be seen for the compound nucleus reaction mechanism beyond the neutron energy of 20 MeV (Fig. 15).

The cross section estimated using the adjusted set of parameters of TALYS for the ^{78}Se(n, p)^{78}As reaction is slightly lower than the measured value (Fig. 16). "ldmodel 2" accounts for the pairing effect and level density enhancement in the odd-odd residual nucleus. Dispersive OMP uses a dispersion relation to connect the real and imaginary parts of the potential. A validated cross section suggests that the model accurately describes the shell-model potential and energies of the bound single-particle states of the target nucleus. Furthermore, "preeq-mode 3" enables the estimation of the pre-equilibrium proton emission close to the neutron energy of 14 MeV. The contribution to the reaction cross section from the compound nucleus mechanism is more than three-fold that of the pre-equilibrium reaction mechanism. Moreover, it can be inferred that the compound reaction mechanism is dominant by 78.80 % over the pre-equilibrium (26.23 %) and direct reaction (4.97 %) mechanisms for the ^{78}Se(n, p)^{78}As reaction. However, the contributions of the pre-equilibrium reaction mechanism and compound reaction mechanism show contradictory trends for neutron energy (E_n) > 15 MeV. The pre-equilibrium contribution gradually increases whereas the contribution of the compound nucleus mechanism reduces after 15 MeV for the ^{78}Se(n, p)^{78}As reaction, as depicted in Fig 16.

The cross section obtained using the adjusted set of parameters for the ^{82}Se(n, $2n$)^{81}Se^{g} reaction shows better agreement with the measured cross section, as depicted in Fig. 17. For the ^{82}Se(n, $2n$)^{81}Se^{g} reaction channel, "ld-model 1" (Constant temperature model) provides a more realistic description of the level density near the neutron separation energy in neutron rich isotopes (^{82}Se). Furthermore, the local Koning-Delaroche OMP ("localomp y") improves the neutron transmission coefficients and normalizes the calculated cross section. The total reaction cross section is dominated by the compound nucleus mechanism, which contributes 100 % at the neutron energy of 14.96 MeV (Table 11). The contribution of the compound nucleus mechanism rises sharply immediately after the threshold energy, and then decreases with increasing neutron energy. However, the direct and pre-equilibrium reaction mechanisms have no contributions to the total cross section for the ^{82}Se(n, $2n$)^{81}Se^{g} reaction. Hence, the theoretical excitation curve reveals only the contribution of the compound reaction mechanism in the

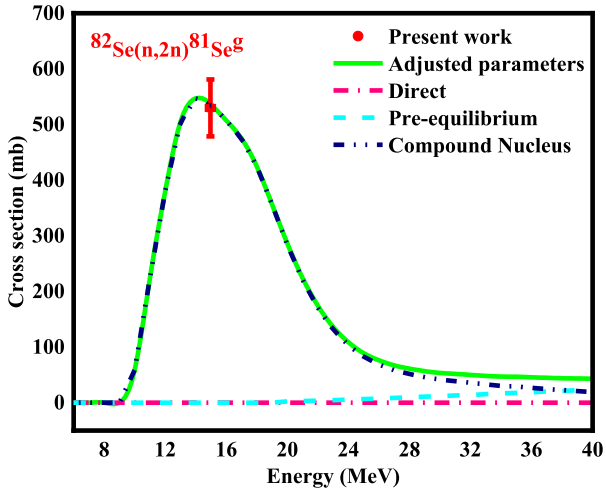

Fig. 17. (color online) Comparison of the measured cross section using the adjusted parameters of TALYS and contribution to the cross section from various reaction mechanisms for the ^{82}Se(n, 2n)^{81}Se^{g} reaction.

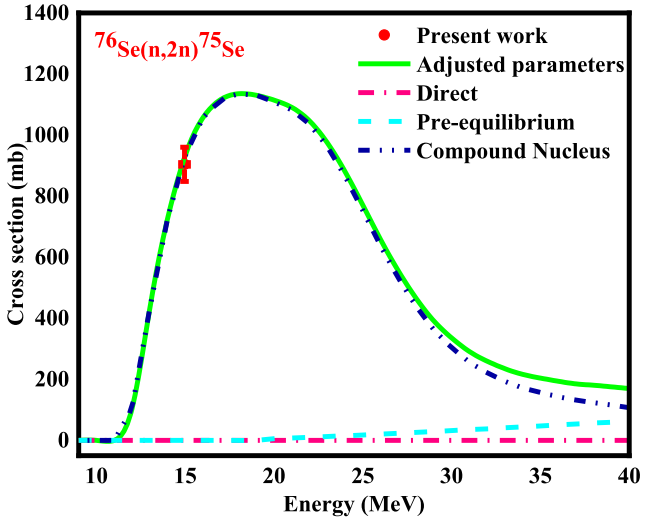

Fig. 18. (color online) Comparison of the measured cross section using the adjusted parameters of TALYS and contribution to the cross section from various reaction mechanisms for the ^{76}Se(n, 2n)^{75}Se reaction.

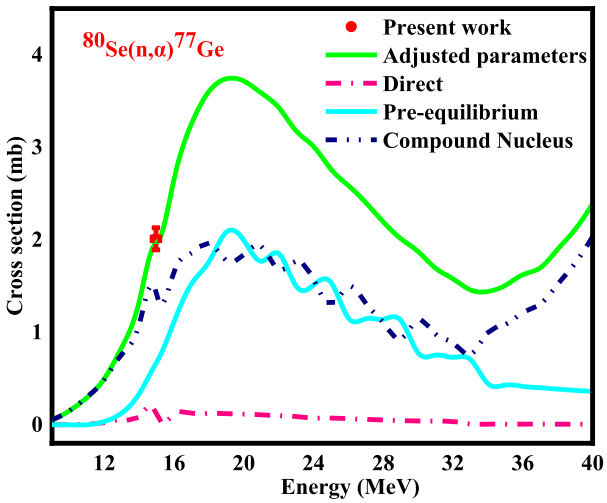

Fig. 19. (color online) Comparison of the measured cross section using the adjusted parameters of TALYS and contribution to the cross section from various reaction mechanisms for the ^{80}Se(n, α)^{77}Ge reaction.

low and intermediate-energy region. At a higher energy (>24 MeV), the contribution of the pre-equilibrium mechanism gradually increases whereas that of the compound nucleus correspondingly decreases, as depicted in Fig. 17.

For the ^{76}Se(n, 2n)^{75}Se reaction, the cross section using the adjusted set of parameters is closely aligned with the measured cross section at the neutron energy of 14.96 MeV. Back-Shifted Fermi Gas model ("ldmodel 2") ensures accurate modeling of the neutron emission probability and incorporates the pairing and shell effects. This suggests that the residual nucleus (^{75}Se) exhibits a statistical compound nucleus behavior with a high density of the excited state. "localomp y" optical model potential optimizes the neutron transmission coefficients, and "preeqmode 3" enhances the description of the pre-equilibrium contributions at higher neutron energies. The theoretical excitation curve representing the contributions of the various reaction mechanisms of the ^{76}Se(n, 2n)^{75}Se reaction is depicted in Fig. 18. At 14.96 MeV, the compound reaction mechanism contributes 100 % to the total cross section, whereas owing to rapid statistical evaporation, the pre-equilibrium and direct reaction mechanisms have zero contributions, as mentioned in Table 11. Furthermore, in the low and intermediate energy regions, the contribution of the compound reaction mechanism is predominant in the ^{76}Se(n, 2n)^{75}Se reaction. However, the pre-equilibrium mechanism fraction starts to increase beyond the neutron energy of 24 MeV (Fig. 18).

The best agreement with the measured cross section is obtained through the adjusted parameters (ldmodel 5, localomp y, preeqmode 1, strength 9, and widthmode 1) for the ^{80}Se(n, α)^{77}Ge reaction. As can be seen in Fig. 19, the cross section obtained using the adjusted parameters increases with increase in the neutron energy up to 15 MeV. The inclusion of "ldmodel 5" provides the description of the spin parity distribution and nuclear structure of the residual nuclei (^{77}Ge) in comparison with the other level density models. Furthermore, "localomp y" refines the neutron entrance and α exit channel transmission coefficients. The excitation curve of the ^{80}Se(n, α)^{77}Ge reaction in the low energy region shows the contribution of the compound nucleus reaction mechanism. The total cross section is predominantly governed by the compound nucleus mechanism (1.43 mb), and is 75.8 % of the total cross section at 14.96 MeV neutron energy. However, the contribution to the total cross section in-

creases for compound nucleus in the higher energy region (beyond 34 MeV). As the neutron energy reaches the intermediate region (~15 MeV), the pre-equilibrium reaction mechanism becomes dominant in the total cross section for the ^{80}Se(n, α)^{77}Ge reaction. Moreover, the contribution of the pre-equilibrium mechanism is approximately 30 % of the total cross section at 14.96 MeV. In contrast, direct reaction has a negligible contribution to the cross section of the ^{80}Se(n, α)^{77}Ge reaction in comparison with those of the other reaction mechanisms from the threshold to 40 MeV neutron energy.

C. Quantification of reaction cross sections using semi-empirical systematic formulae

The semi empirical approach assesses the neutron – induced reaction cross sections using an exponential function, which includes the number of nucleons of the target nucleus. Such a formulation offers a more realistic description of the reaction mechanism, as it comprises both the equilibrium and non – preequilibrium reaction dynamics in the neutron energy range of 13.5−15 MeV [43]. In this study, the established formulae were applied to calculate the (n, p), (n, 2n), and (n, α) reaction cross sections for the Se isotopes, as shown in Tables 12, 13, and 14. Furthermore, a normalized deviation analysis was performed to identify the systematic formulae that best reproduce the experimental data. The measured cross sections of the ^{76}Se(n, p)^{76}As and ^{78}Se(n, p)^{78}As reactions are in concordance with the cross sections estimated by Doczi *et al.* and Levkovski *et al.* by using the systematic formula, respectively. In addition, the measured cross section of the ^{82}Se(n, 2n)^{81}Se^{g} reaction is approximately half the cross section estimated using the empirical systematic formulae. This deviation originates from the mid-shell mass region of the Se isotope. In addition, the semi-empirical formulae rely on the global (N, Z, and A) parameters and do not account for the isomeric and structural properties of the residual nucleus (^{81}Se^{g}). Furthermore, the measured cross section of the ^{76}Se(n, 2n)^{75}Se reaction is aligned with the cross section calculated using the systematic formula of Bychkov *et al.* The cross section of the ^{80}Se(n, α)^{77}Ge reaction, obtained using the systematic formula of Luo *et al.*, exceeds the measured value by approximately 37 %, as shown in Table 14.

VI. CONCLUSIONS

The measured cross sections of the ^{76}Se(n, p)^{76}As, ^{78}Se(n, p)^{78}As, ^{82}Se(n, 2n)^{81}Se^{g}, ^{76}Se(n, 2n)^{75}Se, and ^{80}Se(n, α)^{77}Ge reactions are 55.30 ± 4.09 mb, 18.77 ±

Table 12. Cross sections and normalized deviations using the systematic formulae for the (n, p) reaction cross section, reported by various authors for neutron energies of 13.5−15 MeV.

Authors	Formulae	Mass-region	^{76}Se(n, p)^{76}As		^{78}Se(n, p)^{78}As	
			*σ/mb	§ND	*σ/mb	§ND
Luo [44]	$\sigma_{(n,p)} = 62.98\,(A^{1/3}+1)^2 \exp\left(-34.45\frac{(N-Z)}{A}\right)$	46 ≤ A ≤ 196	45.94	−2.2	21.14	2.1
Forrest [45]	$\sigma_{(n,p)} = 900\,(A^{1/3}+1)^2 \exp(-49.27\frac{(N-Z)}{A} + 197.1\,\frac{(N-Z)^2}{A^2} - 0.45A^{1/2})$	40 ≤ A ≤ 187	24.24	−7.5	21.67	2.5
Habbani [46]	$\sigma_{(n,p)} = 60.34\,(A^{1/3}+1)^2 \exp\left(\frac{-34.44\,(N-Z+1)}{A}\right)$	28 ≤ A ≤ 208	44.07	−2.7	20.28	1.3
Doczi [47]	$\sigma_{(n,p)} = 18.12\,(A^{1/3}+1)^2 \exp\left(\frac{-19.61\,(N-Z)}{A} + \frac{(N-Z)^2}{A^2}\right)$	28 ≤ A ≤ 209	63.74	2.06	41.44	20.2
Kasugai [48]	$\sigma_{(n,p)} = 1264\,(\text{N-Z+1}) \exp\left(\frac{-46.63\,(N-Z+1)}{A}\right)$	28 ≤ A ≤ 187	45.74	−2.4	19.37	0.5
Konno [49]	$\sigma_{(n,p)} = 31.42\,(A^{1/3}+1)^2 \exp\left(\frac{-29.07\,(N-Z)}{A}\right)$	40 ≤ A ≤ 209	40.38	−3.6	21.02	2.0
Ait-Tahar [50]	$\sigma_{(n,p)} = 90.68\,(A^{1/3}+1)^2 \exp\left(\frac{-34.48\,(N-Z+1)}{A}\right)$	40 ≤ A ≤ 187	41.89	−3.2	19.48	0.64
Levkovski [51]	$\sigma_{(n,p)} = 50.21\,(A^{1/3}+1)^2 \exp\left(\frac{-33.8\,(N-Z)}{A}\right)$	40 ≤ A ≤ 209	39.22	−3.9	18.31	−0.4

*Cross section σ (in mb).

§ND denotes the normalized deviation.

Table 13. Cross sections and normalized deviations using the systematic formulae for the (n, $2n$) reaction cross section, reported by various authors for the neutron energies of 13.5−15 MeV.

Authors	Formulae	Mass-region	^{82}Se(n, $2n$)^{81}Se^{g}		^{76}Se(n, $2n$)^{75}Se	
			*σ/mb	§ND	*σ/mb	§ND
Luo [44]	$\sigma_{(n,\,2n)} = 0.0226\,(A^{1/3}+1)^2 \exp\left(\frac{133.86\,(N-Z)}{A} - \frac{779.47\,(N-Z)^2}{A^2} + \frac{1500.51\,(N-Z)^3}{A^3}\right)$	$23 \le A \le 209$	1300.79	14.8	833.05	-1.2
Habbani [46]	$\sigma_{(n,\,2n)} = 20.82\,(A^{1/3}+1)^2 \exp\left(\frac{3.76\,(N-Z+1)}{A}\right)$	$48 \le A \le 238$ A- Even	1183.04	12.7	890.89	-0.2
Chatterjee [52]	$\sigma_{(n,\,2n)} = 31.39\,(A^{1/3}+1)^2 \exp\left(\frac{1.706\,(N-Z)}{A}\right)$	$45 \le A \le 238$	1199.77	13.0	1029.79	2.2
Lu and Fink [53]	$\sigma_{(n,\,2n)} = 45.46\,(A^{1/3}+1)^2 \left[1 - 7.372 \exp\left(\frac{-32.21\,(N-Z+1)}{A}\right)\right]$	$28 \le Z \le 82$	1300.79	15.0	1050.52	2.6
Bychkov [54]	$\sigma_{(n,\,2n)} = 8.7\,(A+100) \left[1 - 0.88 \exp\left(\frac{-7.95\,(N-Z)}{A}\right)\right]$	$45 \le A \le 238$	1547.54	19.8	947.64	0.7

*Cross section σ (in mb).

§ND denotes the normalized deviation.

Table 14. Cross sections and normalized deviations using the systematic formulae for the (n, α) reaction cross section, reported by various authors for neutron energies of 13.5−15 MeV.

Authors	Formulae	Mass-region	^{80}Se(n, α)^{77}Ge	
			*σ/mb	§ND
Luo [44]	$\sigma_{(n,\,\alpha)} = 0.0226\,(A^{1/3}+1)^2 \exp\left(\frac{133.86\,(N-Z)}{A} - \frac{779.47\,(N-Z)^2}{A^2} + \frac{1500.51\,(N-Z)^3}{A^3}\right)$	$23 \le A \le 209$	3.23	10.2
Forrest [45]	$\sigma_{(n,\,\alpha)} = 24.71\,(A^{1/3}+1)^2 \exp(-19.77\,\frac{(N-Z)}{A} + 13.82\,\frac{(N-Z)^2}{A^2} - 0.0248\,A)$	$20 \le Z \le 50$	6.73	39.3
Habbani [46]	$\sigma_{(n,\,\alpha)} = 3.6\,(A^{1/3}+1)^2 \exp\left(\frac{-25\,(N-Z-3)}{A}\right)$	$26 \le A \le 238$ A- Even	6.09	34.0
Kasugai [48]	$\sigma_{(n,\,\alpha)} = 227.86 \exp\left(\frac{-24.66\,(N-Z)}{A}\right)$	$19 \le A \le 202$	5.63	30.2
Ait-Tahar [50]	$\sigma_{(n,\,\alpha)} = 45.46\,(A^{1/3}+1)^2 \exp\left(\frac{-32.75\,(N-Z+1)}{A}\right)$	$40 \le A \le 188$	4.35	19.5
Levkovski [51]	$\sigma_{(n,\,\alpha)} = 16.55\,(A^{1/3}+1)^2 \exp\left(\frac{-31.26\,(N-Z)}{A}\right)$	$31 \le A \le 202$	4.28	18.9
Csikai [55]	$\sigma_{(n,\,\alpha)} = 15.07\,(A^{1/3}+1)^2 \exp\left(\frac{-25.98\,(N-Z)}{A} + \frac{(N-Z)^2}{A^2}\right)$	$19 \le A \le 202$	8.81	56.7

*Cross section σ (in mb).

§ND denotes the normalized deviation.

1.12 mb, 529.78 ± 51.23 mb, 903.98 ± 55.99 mb, and 2.01 ± 0.12 mb, respectively. The measured cross sections with minimum statistical uncertainty are consistent with the previously reported data (EXFOR). However, the cross section of the ^{82}Se(n, $2n$)^{81}Se^{g} reaction exceeds the latest reported data of A. A. Filatenkov *et al.* by approximately 29.7 %. The measured cross sections are consistent with the excitation curve of the evaluated library data. Across all level density models, the (n, $2n$) reaction cross sections are significantly higher than those of the other reaction channels at the neutron energy of 14.96 MeV. Furthermore, most of the studied reaction channels were adequately reproduced using the adjusted (optimal) set of parameters, except for the ^{78}Se(n, p)^{78}As reaction.

In addition, the γ ray SFM, *i.e.*, strength 1 and strength 2, employed for the ^{82}Se(n, $2n$)^{81}Se^{g} and ^{76}Se(n, $2n$)^{75}Se reactions, respectively, were modified. Despite this, only the measured cross section for the ^{80}Se(n, α)^{77}Ge reaction is in concordance with that obtained using the semi- empirical systematic formulae of Luo *et al*. Therefore, the precise measurements of the cross sections for the selected isotopes of Se could significantly enhance the accuracy of the calculations using the statistical model and semi- empirical systematic formulae, thus contributing to more robust future evaluations.

ACKNOWLEDGMENT

The authors are thankful to the personnel of the Fusion Blanket Division, IPR, for the sample preparation, and personnel of the Neutron and Ion Irradiation Facility (NIIF) for their support and guidance throughout the experiment. One of the authors (Vandana) thanks the NSUT for providing the fellowship.

References

[1] E. Curti, A. Puranen, D. Grolimund *et al*., Environ. Sci. : Processes Impacts **17**, 1760 (2015)
[2] K. J. Weeks, R. J. Schulz, Med. Phys. **13**, 728 (1986)
[3] M. Upadhyay, Choudhary M, Singh N *et al*. , J. of Phys. G: Nucl. Part. Phys. **50**, 125107 (2023)
[4] A. Hingu *et al*., Chin. Phys. C **48**, 024001 (2024)
[5] S. Parashari *et al*., Eur. Phys. J. A **55**, 51 (2019)
[6] M. Abhangi, S. Vala, H. L. Swami *et al*., Fusion Eng. Des. **204**, 114522 (2024)
[7] S. Vala, R. Kumar, M. Abhangi *et al*,, Fusion Eng. Des. **217**, 115158 (2025)
[8] L. F. Curtis, *Introduction to Neutron Physics* (Princeton: D. Van Nostrand Company, 1969)
[9] J. Luo, L. Du, and J. Zhao, Instrum. Methods Phys. Res. Sect. B **298**, 61 (2013)
[10] T. Vidmar, Nucl. Instrum. Methods Phys. Res. A **550**, 603 (2005)
[11] N. Otuka, B. Lalremruata, M. Khandaker *et al*., Radiat. Phys. Chem. **140**, 502 (2017)
[12] L. P. Geraldo, D. L. Smith, Nucl. Instrum. Methods Phys. Res. A **290**, 499 (1990)
[13] M. Karkera *et al*. 2018 Internal report No. MAHE/STATISTICS/DAE-BRNS/2018/4
[14] R. K. Singh, N. L. Singh, R. D. Chauhan *et al*., Chin. Phys. C **46**, 054002 (2022)
[15] Vandana, S. Sharma, P. Bangotra *et al*. , J. Radioanal. Nucl. Chem. **334**, 7537 (2025)
[16] Vandana, S. Sharma, in *2025 25th Int. Sci. Conf. Electr. Power Eng. (EPE)* (Prague: IEEE, 2025)
[17] A. Trkov *et al*., Nucl. Data Sheets **163**, 1 (2020)
[18] D. W. Millsap, and S. Landsberger, Appl. Radiat. Isot. **97**, 21 (2015)
[19] J. Luo, F. Tuo, X. Kong *et al*., Annals of Nucl. Energy **36**, 718 (2009)
[20] S. Sharma, Vandana, P. Bangotra *et al*., Appl. Radiat. Isot. **220**, 111758 (2025)
[21] D. L. Smith, J. W. Meadows, P. A. Moldauer *et al*., Nucl. Phys. A **388**, 37 (1982)
[22] T. S. Ganesapandy, G. T. Bholane, S. H. Patil *et al*., Radiat. Phys. Chem. **212**, 111101 (2023)
[23] A. A. Filatenkov, IAEA Nuclear Data Section Report No. INDC(CCP)-0460 (Vienna, Austria, 2016)
[24] A. J. Koning *et al*. , J. Korean Physical Soc. 59, 1057 (2011)
[25] Z. Ge, R. Xu, H. Wu *et al*., EPJ Web Conf. **239**, 09001 (2020)
[26] J. Luo, X. Xu, X. Cao *et al*., Nucl. Instrum. Methods in Phys. Res. B **265**, 453 (2007)
[27] H. M. Hoang, U. Garuska, A. Marcinkowski *et al*., Zeitschrift Fuer Physik A Hadrons and Nuclei **334**, 285 (1989)
[28] A. J. Koning, D. Rochman, J. Sublet *et al*., Nucl. Data Sheets **155**, 1 (2019)
[29] G. He, Z. Liu, J. Luo *et al*., Indian J. Pure and Appl. Phys. **43**, 729 (2005)
[30] O. Iwamoto, N. Iwamoto, S. Kunieda *et al*., J. Nucl. Sci. Technol. **60**, 1 (2023)
[31] J. Luo, L. He, Eur. Phys. J. A **61**, 30 (2025)
[32] A. J. Koning, S. Hilaire, S. Goriely, Eur. Phys. J. A **59**, 131 (2023)
[33] S, Sharma *et al*., Radiat. Phys. Chem. **244**, 113746 (2026)
[34] Vandana, S. Sharma *et al*., Eur. Phys. J. Plus, **141**, 253 (2026)
[35] A. V. Ignatyuk, K. K. Istekov, and G. N. Smirenkin, Sov. J. Nucl. Phys. **29**, 450 (1979)
[36] M. Mehta, N. L. Singh, R. Singh *et al*. , J. Radioanal. Nucl. Chem. **333**, 5231 (2024)
[37] S. Sharma, Vandana *et al*., in *2025 25th International Scientific Conference on Electric Power Engineering (EPE)*(Piscataway: IEEE, 2025)
[38] A. V. Ignatyuk, J. L. Weil, S. Raman *et al*., Phys. Rev. C **47**, 1504 (1993)
[39] J. Kopecky and M. Uhl, Phys. Rev. C **41**, 764 (1976)
[40] A. V. Ignatyuk, G. N. Smirenkin, and A. S. Tishin, Sov. J. Nucl. Phys. **21**, 255 (1975)
[41] S. Goriely, F. Tondeur, and J. M. Pearson, Atom. Data Nucl. Data Tables **77**, 311 (2001)
[42] S. Hilaire, S. Goriely and A. J. Koning, Phys. Rev. C **86**, 064317 (2012)
[43] A. Hingu *et al*., Radiat. Phys. Chem. **188**, 109634 (2021)
[44] J. Luo, F. Tuo. F. Zhou *et al*., Nucl. Instrum. Methods. Phys. Res. B **266**, 4862 (2008)
[45] R. A. Forrest and J. Kopecky, Fusion Eng. Des. **82**, 73 (2007)
[46] F. I. Habbani and K. T. Osman, Appl. Radiat. Isot. **54**, 283 (2001)
[47] R. Doczi, V. Semkova *et al*. , IAEA-NDS Report No. Indc (HUN)-032 (Vienna, Austria, 1997)
[48] Y. Kasugai, Y. Ikeda, H. Yamamoto *et al*., Measurement of activation cross sections for mercury isotopes in the neutron

energy range between 13.4 and 14.9 MeV, in *Proceedings of the 1994 symposium on nuclear data* (Tokai: Japan Atomic Energy Research Institute, 1995), JAERI-Conf-95-008

[49] C. Konno, Y. Ikeda, K. Oishi *et al*., Activation cross section measurements at neutron energy from 13.3 to 14.9 MeV, (Tokai: Japan Atomic Energy Research Institute, 1993), JAERI Report No. 1329

[50] S. Ait-Tahar, J. Phys. G: Nucl. Phys. **13**, L121 (1987)

[51] V. N. Levkovski, Zh. Eksp. Teor. Fiz. **45**, 305 (1963)

[52] S. Chatterjee and A. Chatterjee, Nucl. Phys. A **125**, 593 (1963)

[53] W. Lu and R. W. Fink, Phys. Rev C **4**, 1173 (1971)

[54] V. M. Bychkov, V. N. Manokhin *et al*. , INDC (CCP)-146, IAEA-NDS (Vienna, Austria, 1980)

[55] J. Csikai, V. Semkova, R. Doczi *et al*., Fusion Eng. Des. **37**, 65 (1997)